Kinetic Modeling of the Reaction between Hydrated Lime and SO_2 at Low Temperature

M. Bausach, M. Pera-Titus, C. Fité, F. Cunill, J.-F. Izquierdo, J. Tejero, and M. Iborra
Dept. of Chemical Engineering and Metallurgy, University of Barcelona, Barcelona 08028, Spain

DOI 10.1002/aic.10403
Published online March 28, 2005 in Wiley InterScience (www.interscience.wiley.com).

The kinetics of the noncatalytic solid–gas reaction between $Ca(OH)_2$ and SO_2 at low temperature and in the presence of water vapor was investigated. The effect of relative humidity, temperature, and SO_2 concentration on the desulfurization capacity of the solid was evaluated, as well as the effect of NO_2 concentration. A deactivation model (DM) and a new version of this model, by implementing an inverse shrinking core model (DM-ISCM) with an ionic solid-state diffusion control, were fitted to experimental kinetic data. The proposed model showed the best agreement with the experimental results. A chemical mechanism for the reaction on the solid surface was also discussed. © 2005 American Institute of Chemical Engineers *AIChE J,* 51: 1455–1466, 2005
Keywords: SO_2, $Ca(OH)_2$, NO_2, desulfurization, hydroxide lime, deactivation model, solid- state diffusion

Introduction

Because of the increasing social and political concern with respect to the atmospheric environment, research on air purification has been on the increase in the last few decades because air quality control and regulations against hazardous pollutants have become stricter in many countries. In this way, a number of new technologies have been developed to capture acidic gaseous pollutants (mainly SO_2 and NO_x) emitted from coal combustion in first-generation power plants. Special attention has been paid to recovery of SO_2, given its role in generation of acidic rain. Nowadays, flue gas desulfurization (FGD) processes, which are based on the injection of Ca-based sorbents, are well-established technologies. The sorbents, basically CaO, $CaCO_3$, or $Ca(OH)_2$, can be either introduced directly into the furnace or sprayed or injected as a slurry into the duct placed between the air preheater and the particulate collection system.[1]

The noncatalytic solid–gas reaction of Ca-based sorbents with SO_2 at common furnace temperatures (700–1100°C) has been the focus of previous extensive and fundamental research. The aim of reducing operating temperatures has led more recently to the development of applications in the presence of water vapor. At low temperatures and in the presence of water vapor, the primary reaction that has been traditionally proposed in an FGD process is as follows[2]:

$$Ca(OH)_2 + SO_2 \xrightarrow{H_2O} CaSO_3 \cdot (1/2)H_2O + (1/2)H_2O \quad (1)$$

Numerous studies have been devoted to describing mathematically the kinetics of the reaction between Ca-based sorbents and SO_2 at high temperatures and for large particles (100–3000 μm). The kinetic models proposed can be grouped as: (1) grain models,[3-7] (2) pore models,[8-11] (3) volume reaction models,[12] and (4) deactivation models.[13,14]

However, only a few studies concerning the kinetics of the reaction between $Ca(OH)_2$ and SO_2 at low temperatures and in the presence of water vapor can be found in the literature. This process is characterized by a sharp decrease of the reaction rate with solid conversion (the reaction rate decreases about two orders of magnitude when the solid conversion reaches 5% operating at 50% of relative humidity[15]) and by an incomplete solid conversion. The studies surveyed in the literature all agree with the great impact of relative humidity (RH) on both the solid conversion[2,16-18] and the reaction rate.[15] Whereas

Correspondence concerning this article should be addressed to F. Cunill at cunill@angel.qui.ub.es.

© 2005 American Institute of Chemical Engineers

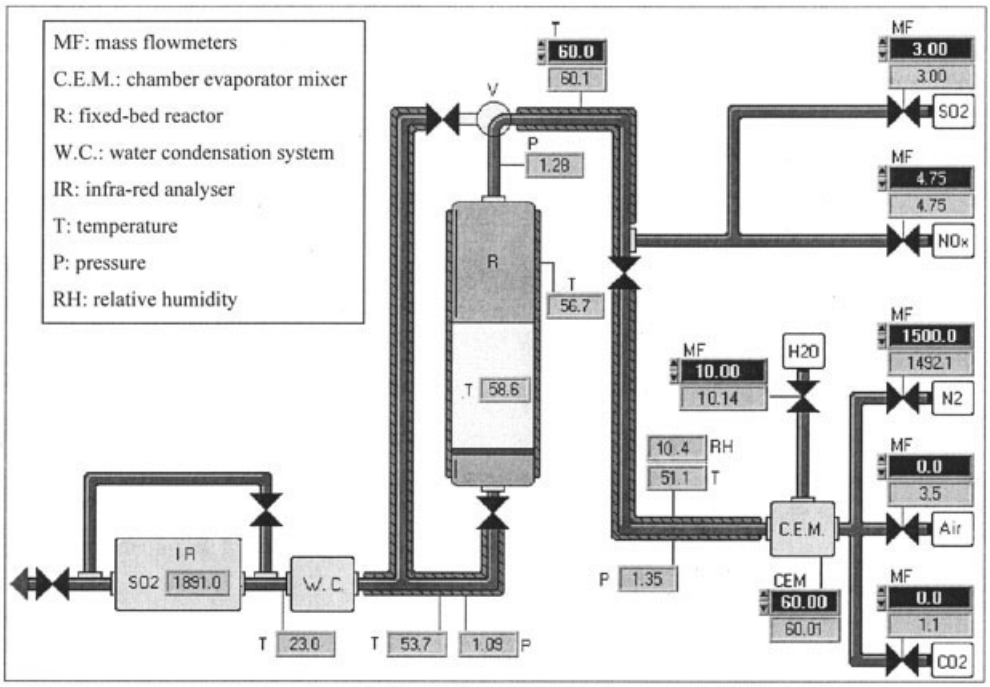

Figure 1. Experimental setup.

Yoon et al.[19] detected a positive effect of RH on the initial solid reactivity, Rochelle et al.[16] observed a moderate effect at very short times. Experimental data reported[2,15,20] at RH $>$ 70% appear to show that the reaction does not stop at long times (after 1 h), even though the reaction rate has already dramatically decreased. On the other hand, the effect of NO_2 on the kinetics of this reaction has rarely been studied. When done, it has been reported that NO_2 enhances the recovery of SO_2 both in a baghouse and in a fixed-bed reactor by means of the formation of some nitrate and nitrite species.[21-23]

Because the experimental kinetic behavior cannot be described by means of the simplest form of the shrinking core model (SCM),[24] several attempts have been made to develop empirically improved versions of this model, by taking into account either improved effective diffusion coefficients or effective surface areas with a decreasing exponential dependency on conversion.[2,17] Another model based on the adsorption of SO_2 on a nonideal solid surface as the rate-limiting step was proposed,[25] where the adsorption activation energy is assumed to depend linearly on the surface coverage. More recently, a deactivation model (DM) was adapted to experimental data with a reaction rate proportional to the fraction of active surface area not covered by the product.[26]

Krammer et al.[15] suggested the presence of four stages with different prevailing mechanisms during the reaction:

(1) The formation of a product monolayer, mainly determined by both the SO_2 concentration and the RH.

(2) The formation of consecutive product layers, depending mostly on the RH.

(3) A product layer diffusion, becoming the rate-limiting step with a reaction rate affected only by the RH and a reaction product that is thought to be built up in a *clusterlike* form at a high RH, which could result in a better accessibility of the still unreacted material.

(4) Pore closure, which could explain the significant decrease of the reaction rate at high conversions.

Klingspor et al.[27] also proposed a reaction mechanism based on the preferential retention of SO_2 in the presence of adsorbed water, where the formation of a hydrated complex of SO_2 on the solid surface could be the rate-limiting step, and a higher RH would involve the formation of more stable compounds.

The analysis of the structural properties of the solids at different reaction times, carried out by Ortiz et al.,[28] supported the conclusion that the region of 9–200 nm is the effective pore size for the desulfurization reaction. They also found a linear decrease of the surface area and the pore volume of the solid with conversion because the molar volume of the product is higher than that of the reagent (in a ratio of 1.5). This result was later confirmed by Ho et al.[26] Furthermore, Krammer et al.[15] and Ho et al.[26] found that conversion per BET (Brunauer–Emmett–Teller) unit area was irrespective of particle size in the diameter range between 50 and 120 and 10 and 96 μm, respectively.

The aim of the present article is the study of the reaction between $Ca(OH)_2$ and SO_2 at low temperature, evaluating the effect of RH, temperature, and the presence of NO_2 on SO_2 breakthrough curves obtained in a fixed-bed reactor. A kinetic model is proposed to fit experimental data and a chemical mechanism for the reaction is also suggested.

Experimental Setup and Procedure

Experiments were carried out in the setup depicted schematically in Figure 1. The equipment consists of a continuous feeding system, a fixed-bed reactor, a continuous analytical system [infrared (IR) instrument], and a personal computer equipped with LabVIEW® software. Synthetic flue gas, to simulate the gas emitted by power plants, was obtained by

Table 1. Experimental Conditions

Total flow (NmL min^{-1})	1500
SO_2 inlet concentration (ppm)	2000–8000
NO_2 inlet concentration (ppm)	72–250
RH (%)	0–70
Reaction temperature (°C)	40–80
$Ca(OH)_2$ weight (g)	1.0
Inert weight (g)	30
Experimental times (h)	1–3

feeding the appropriate amount of pure gases (SO_2 and N_2) and N_2/NO_2 mixtures from pressurized gas cylinders. The steam feed was obtained by using a controlled evaporator mixer (CEM), equipped with a liquid mixing valve to control the water flow rate. The reactor consists of a jacketed Pyrex® tube (450 mm height, 12 mm ID) packed with a mixture of $Ca(OH)_2$ and sea sand (SiO_2) (weight ratio of 1:30 and apparent porosity of 23%), to avoid the channeling of the gas and to ensure isothermal conditions. The concentration of SO_2 at the outlet was continuously monitored by means of an IR instrument.

The experimental conditions checked in this work are summarized in Table 1. In the progress of an experiment, the N_2 stream with the required humidity is led to the reactor, and after 5 min, the required flows of the other components are supplied. Preliminary tests were carried out to ensure that the preconditioning time would not affect the results. Breakthrough curves of SO_2 concentration in the gas stream leaving the reactor are plotted. The total amount of SO_2 removed from the flue gas in one experiment can be calculated from the difference between the area associated with a breakthrough curve and the one corresponding to a breakthrough blank curve. The reliability of this method was verified by determining the S/Ca ratios of the reacted solid through X-ray fluorescence (XRF) analysis and comparing it with the results of the breakthrough curves (see Table 2). In addition, to identify the product formed, X-ray diffraction (XRD) analysis of the reacted solid was carried out and, to verify whether nitrite and nitrate ions are formed when the reaction takes place in the presence of NO_2, some exploratory analyses were also done using ion chromatography (IC).

The main properties of the reagent and the inert solid used in this work are listed in Table 3. The reagent is a powder of $Ca(OH)_2$ of high purity and low porosity, supplied by Ciaries Co. (Barcelona, Spain), and the inert solid is a commercial sea sand (SiO_2) (Fluka, Buchs, Switzerland). BET surface area and porous distribution of reagent particles were determined by nitrogen desorption at 77 K (see Figure 2), and their morphology was examined by SEM analysis. As can be seen in Figure 3, particles are irregular in shape and seem to be agglomerates of an average size of 10 μm assembled from small 1-μm subparticles.

Table 3. Main Properties of the Solids

$Ca(OH)_2$	
Composition*	~99% $Ca(OH)_2$
	<1% $CaCO_3$
	<0.05 g X/g Ca**
Particle diameter† (mean) (μm)	9.4
BET specific surface ($m^2\ g^{-1}$)	13.8 ± 0.1
Pore volume ($cm^3\ g^{-1}$)	0.060
Porosity (%)	14
Pore diameter (mean) (nm)	17.5
Inert solid: sea sand (SiO_2)	
Composition	>99.9% SiO_2
Particle diameter† (mean) (μm)	308

*Determined by X-ray diffraction.
**X: Si + Mg + Al + S + K + Fe + Na + P.
†Determined by laser diffraction granulometry.

Theory

Reactor modeling

The integral fixed-bed reactor used in this work may be modeled by means of a set of two microscopic mass balances for both the solid and gas reagents. A plug-flow regime can be assumed, given that the criteria $D/d_p > 30$ and $L/d_p > 100$ are attained,[29,30] where D and L correspond to the diameter and height of the bed, respectively, and d_p is the diameter of the inert solid particles. Thus, the equation set takes the following general form:

Gas Balance

$$\frac{\varepsilon_L}{\rho_S(1-\varepsilon_L)}\frac{\partial C_g}{\partial t} = \frac{-1}{\rho_S(1-\varepsilon_L)}\frac{\partial(\nu C_g)}{\partial z} - r_g \qquad (2)$$

Solid Balance

$$\frac{1}{M_S}\frac{dX_S}{dt} = r_S \qquad (3)$$

with the initial condition $t = 0$, $\forall z$, C_g, and $X_S = 0$ and the boundary condition $z = 0$, $\forall t$, $C_g = C_g^0$, where ρ_S, M_S, and X_S correspond to the density, the molecular weight, and the conversion of the solid reagent, respectively; ε_L is the porosity of the bed; ν is the speed of the gas in the bed; C_g and C_g^0 represent the gas concentrations in the bed and at the inlet, respectively; and r_g and r_S indicate the reaction rate of the gas and solid reagents, respectively, which are related stoichiometrically by Eq. 1. Moreover, Eq. 2 can be assumed to be pseudo-steady, taking into account the approximation, $\partial C_g/\partial t \ll \partial(\nu C_g)/\partial z$.

Table 2. SO_2 Retention Determined from Gas-Phase Analyses*

% RH	C_{SO2} (ppm)	C_{NO2} (ppm)	Reaction Time (h)	mol SO_2/mol Ca (by IR)	mol SO_2/mol Ca (by XRF)**
60	1100	0	1	0.1216 ± 0.0061	0.1284 ± 0.0051
60	2000	0	1	0.225 ± 0.013	0.2017 ± 0.0062
70	2000	0	1	0.254 ± 0.016	0.2035 ± 0.0096
30	2000	175	1	0.132 ± 0.011	0.1367 ± 0.0058
50	2000	175	2	0.327 ± 0.018	0.3218 ± 0.0094
60	2000	175	2	0.635 ± 0.023	0.529 ± 0.013

*All experiments were carried out at 333 K.
**Error inlcudes only fluorescence analysis error.

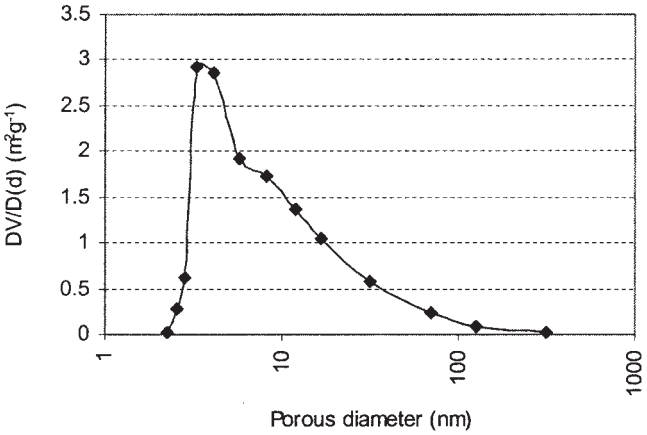

Figure 2. Pore-size distribution of $Ca(OH)_2$.

Kinetic model

First of all, the following aspects related to mass transfer in the particles have been taken into account:

(1) External mass transfer coefficients have been estimated in the range 300–600 m s^{-1}, and therefore external mass transfer can be neglected, in agreement with Ruiz-Alsop and Rochelle[2] for similar operating conditions.

(2) Intraparticle mass transfer can be neglected, as has been experimentally confirmed in previous studies with particles of similar size.[15,26]

The exploratory screening of different models to describe the experimental kinetic data obtained has been focused on two consecutive steps. First, a deactivation model, already applied in the literature at low temperature, has been tested. Afterward, a modified version of this model has been evaluated to improve the fitting to experimental data.

Deactivation model

A deactivation model (DM) assumes that the reaction between the gas molecules and the solid reagent depends mainly on the concentration of the gas on the solid surface and on the so-called active surface (a_S), that is, the ratio of active surface of unreacted solid and the initial solid surface (S_S/S_S^0). As the reaction progresses, the solid product deposits on the surface of the reagent and the solid activity becomes reduced. Thus, the reaction rate can be expressed in the same manner as that reported by Doğu et al.[31]

$$r_S = \frac{\varepsilon_L}{\rho_S(1-\varepsilon_L)} k_S C_g^n a_S \tag{4}$$

where k_S and n indicate the rate constant and the reaction order with respect to the gas concentration, respectively. Furthermore, the rate of reduction of active surface—or deactivation rate—is thought to depend on the activity of the solid and on the gas concentration in a way that is commonly proposed for the deactivation of catalysts,[32] as follows

$$\frac{da_S}{dt} = -\beta C_g^m a_S \tag{5}$$

where m is the order of the deactivation process with respect to the gas concentration, with typical values of 0 or 1,[31] and β is the deactivation rate constant. The integration of Eq. 5 for $m = 0$ and for $m \neq 0$ and C_g^m constant with the initial condition $t = 0$, $a_S = 1$ and its subsequent combination with Eq. 4 yields the following general expression

$$r_S = \frac{\varepsilon_L}{\rho_S(1-\varepsilon_L)} k_S C_g^n \exp(-\beta C_g^m t) \tag{6}$$

which indicates that at long times, when the activity of the solid becomes zero, the reaction rate also tends to zero because no active surface area is left. In the case $m \neq 0$ and C_g^m is not constant, no analytical expression for the r_S can be found and the concentrations and active surface must be calculated separately.

Deactivation model combined with an inverse shrinking core model (DM-ISCM)

The aforementioned DM takes into account just the contribution of the remaining active surface area of the solid reagent to the reaction rate. However, one can assume that other parallel pathways might take place simultaneously with the deactivation of the surface. While the reaction goes on and a thin layer of the solid product covers partially the reagent surface, further reaction controlled by a slow diffusional process in this layer may be suggested, as discussed below.

Because SO_2 concentration has no significant influence on the reaction rate at long times (after a few minutes) at low temperatures and in the presence of water,[15,16,33] because hydrated SO_2 is a very large molecule (kinetic diameter of SO_2 = 2.3 Å), and because the product of similar desulfurization reactions at high temperatures are usually nonporous,[31] the diffusion of SO_2 through the product layer should not account for the progression of the reaction. However, an outward solid-state diffusion of hydrated Ca^{2+} and HO^- ions from the inner $Ca(OH)_2/CaSO_3{\cdot}(1/2)H_2O$ interface to the outer $CaSO_3{\cdot}(1/2)H_2O$/gas surface could take place together with the deactivation of the surface of $Ca(OH)_2$. In fact, the studies done by Hsia et al.[34], who used platinum markers and a *two-stage* sulfation technique with $^{32}SO_2$ and $^{34}SO_2$, showed that an

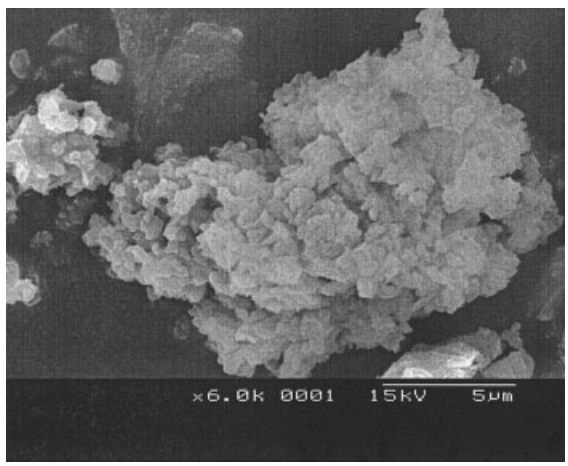

Figure 3. SEM micrograph of $Ca(OH)_2$.

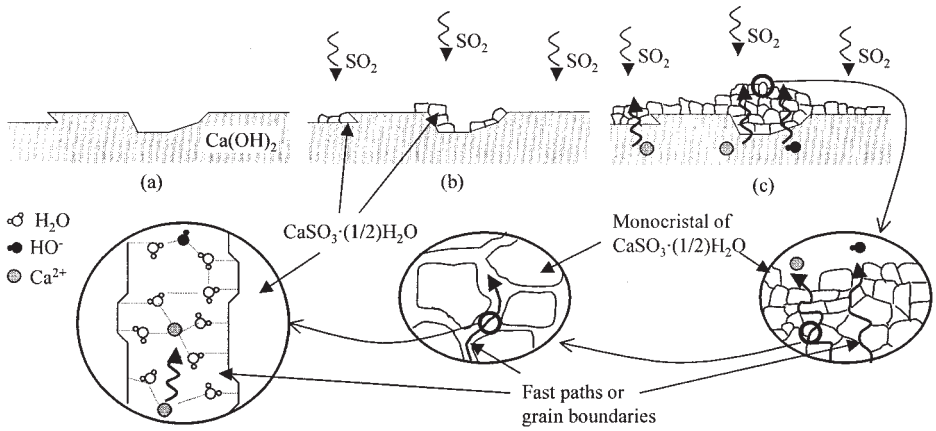

Figure 4. Representation of the evolution of the surface.

(a) Unreacted surface; (b) surface partially deactivated by the covering of product crystals; (c) deactivated surface and predominance of outward solid-state diffusion of Ca^{2+} and HO^- ions. Diffusion through grain boundaries is likely promoted by the effect of adsorbed water.

outward solid-state diffusion mechanism occurs, at least at high temperatures.

The ionic diffusion through crystals may occur mainly by means of two mechanisms: (1) *lattice diffusion* or jumps between near Schottky and Frenkel thermally induced lattice vacancies in the crystals, and (2) *grain boundary diffusion* or jumps between active sites in crystal boundaries. Because of the much lower activation energy for boundary diffusion, it is dominant at low temperature, whereas lattice diffusion is more relevant as the temperature increases.[35] Consequently, it should be considered that the contribution of mechanism (2) in the ionic diffusion through the $CaSO_3{\cdot}(1/2)H_2O$ layer is predominant at low temperatures. On the other hand, given that solid-state diffusion is related to the nature of the involved compounds, the ion-transfer mechanism should be altered by the presence of adsorbed substances or impurities. In this way, it is plausibly proposed that the adsorbed water both on the grain boundaries and in the bulk of the crystals might reduce the activation energy of the jumps, and therefore adsorbed water might enhance the ion diffusion, as illustrated in Figure 4.

The ionic mass transfer through a layer can be modeled by means of the Nernst–Planck equation,[36] which considers that the driving force for ionic diffusion is ascribed to two contributions: (1) the ionic concentration gradient through the layer; and (2) the electrical field gradient in the layer, which should be caused by a net charge in each side of the layer. The general formulation of this equation for the transfer of the ion **i** through the product layer (*P*), neglecting any coupling phenomenon with the transfer of other ions **j**, is as follows

$$\vec{J}_i = -\left[D_i^P \vec{\nabla} C_i^P + z_i D_i^P C_i^P \frac{F}{RT} \vec{\nabla} \phi^P \right] \tag{7}$$

where C_i^P, D_i^P, and z_i correspond to the concentration, the solid-state diffusion coefficient, and the electric charge of ion i in the product layer, respectively; ϕ^P is the electric field in the product layer; and F is the Faraday constant. The condition of electrical neutrality requires the following relation to be fulfilled

$$\vec{J} = \sum_i z_i \vec{J}_i = 0 \tag{8}$$

which leads to the expression

$$\vec{J}_i = -\bar{D}_i^P \nabla C_i^P \tag{9}$$

which is analogous to Fick's first law, with a diffusion coefficient for species **i** ($\bar{D}_i^P$) that includes the drift of all the ionic species, defined as follows for two of them

$$\bar{D}_i^P = \bar{D}_j^P = \frac{(z_i^2 x_i + z_j^2 x_j) D_i^P D_j^P}{z_i^2 x_i D_i^P + z_j^2 x_j D_j^P} \tag{10}$$

where x_i and x_j are the molar fraction of species i and j, respectively. Under the assumption that the concentration of both ions (Ca^{2+}, HO^-) is null on the outer surface of the solid product, derived from considering ionic transfer control, the electric field gradient in the product layer also should be null. Equation 9 can be solved by taking into account the following assumptions:

(1) The product layer is approximately continuous (see Figure 4c).

(2) Aggregation between particles is negligible.

(3) The particles are spherical.

(4) The concentration of free Ca^{2+} and HO^- ions in the $Ca(OH)_2/CaSO_3{\cdot}(1/2)H_2O$ interface is considered to correspond, respectively, to their values in the crystalline lattice of $Ca(OH)_2$.

Then, the surface flow of both ions, $J_{Ca^{2+}}$ and J_{HO^-}, may be described by the following expression

$$J_{Ca^{2+}} = \frac{1}{2} J_{HO^-} = \frac{3}{R^2 \rho_S} \frac{\bar{D}_{Ca^{2+}}^P C_{Ca}^R}{(1 - X_S)^{-1/3} - 1} \tag{11}$$

where C_{Ca}^R is the concentration of Ca^{2+} ions in the crystalline lattice of $Ca(OH)_2$ (3.2×10^{-2} mol cm^{-3}) and R is the radius

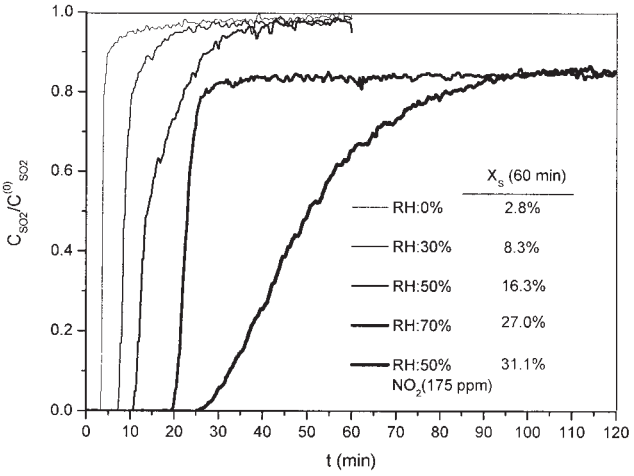

Figure 5. Influence of RH and NO_2 on SO_2 breakthrough curves at 60°C and 2000 ppm SO_2.

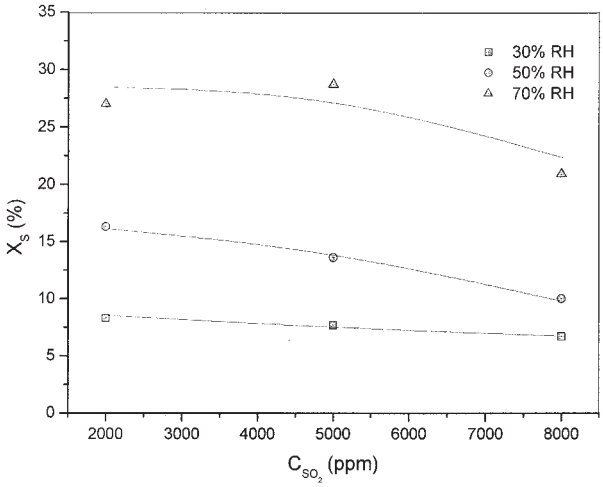

Figure 7. Influence of SO_2 on X_S after 1 h of reaction at 60°C.

of the spherical particles. Equation 11 is analogous to the SCM, which has been traditionally proposed for an inward controlling diffusion of a gas reagent.[37] Finally, the combination of Eqs. 4 and 11 gives the final general expression for r_S for the DM-ISCM

$$r_S = \frac{\varepsilon_L}{\rho_S(1-\varepsilon_L)} k_S C_g^n a_S + \frac{3}{R^2\rho_S} \frac{\bar{D}^P_{Ca^{2+}} C^R_{Ca}}{(1-X_S)^{-1/3}-1} \quad (12)$$

In the case $m = 0$ and $m \neq 0$ with C_g^m constant, the final expression for r_S is transformed as follows by combining Eqs. 6 and 11

$$r_S = \frac{\varepsilon_L}{\rho_S(1-\varepsilon_L)} k_S C_g^n \exp(-\beta C_g^m t) + \frac{3}{R^2\rho_S} \frac{\bar{D}^P_{Ca^{2+}} C^R_{Ca}}{(1-X_S)^{-1/3}-1} \quad (13)$$

Equation 12 can be rewritten as follows

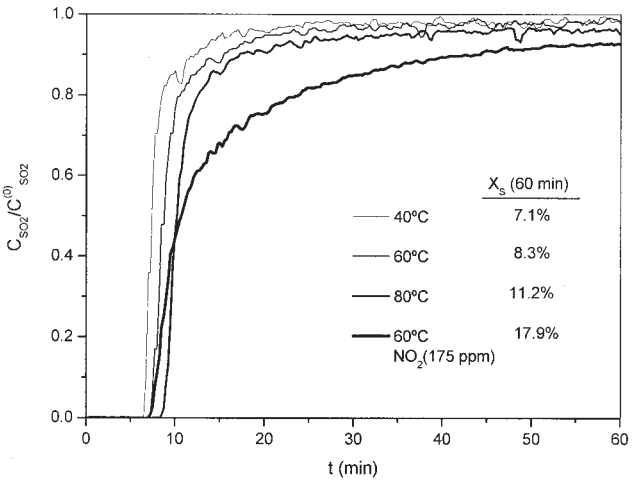

Figure 6. Influence of *T* and NO_2 on SO_2 breakthrough curves at 30% RH and 2000 ppm SO_2.

$$r_S = \Phi k_S C_g^n a_S + \Psi \bar{D}^P_{Ca^{2+}} \left[\frac{1}{(1-X_S)^{-1/3}-1} \right] \quad (14)$$

where $\Phi = \varepsilon_L/[\rho_S(1-\varepsilon_L)]$ and $\Psi = 3C^R_{Ca}/R^2\rho_S$, respectively. As a result, the model contains three adjustable parameters to be fitted to the experimental results: k_S, β, and $\bar{D}^P_{Ca^{2+}}$.

Model fittings

The following sets of equations have been fitted to the experimental kinetic results in the fixed-bed reactor:

(1) $n = 0$, $n = 1$, and $m = 0$ in DM $\Rightarrow$ Eqs. 2 + 3 + 6

(2) $n = 0$, $n = 1$, and $m = 1$ in DM $\Rightarrow$ Eqs. 2 + 3 + 4 + 5

(3) $n = 0$, $n = 1$, and $m = 0$ in DM-ISCM $\Rightarrow$ Eqs. 2 + 3 + 13

(4) $n = 0$, $n = 1$, and $m = 1$ in DM-ISCM $\Rightarrow$ Eqs. 2 + 3 + 5 + 12

Each set of equations has been solved numerically by using a spatial and temporal discretization through the finite-difference method. A least-square nonlinear optimization method, based on the Levenberg–Marquardt algorithm, was used to adjust the kinetic parameters β, Φ, and Ψ by comparison of the predicted and the experimental breakthrough curves at the outlet of the reactor. The confidence interval of the fitted kinetic parameters was calculated by means of a standard method for nonlinear models.[38]

Results

Experimental SO_2 breakthrough curves

The influence of the RH and temperature (T) on the breakthrough curves is shown in Figures 5 and 6, where the values of the solid conversion at exposure times of 60 min are also indicated. A positive effect of the RH and a slight influence of

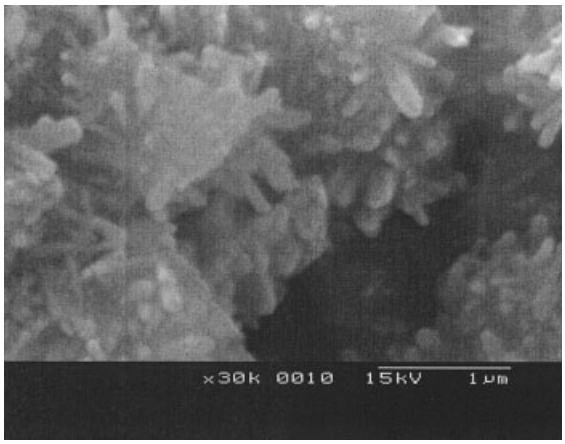

Figure 8. SEM micrograph of $Ca(OH)_2$ reacted with 2000 ppm SO_2 at 75% RH, 60°C, time of exposure: 3 h.

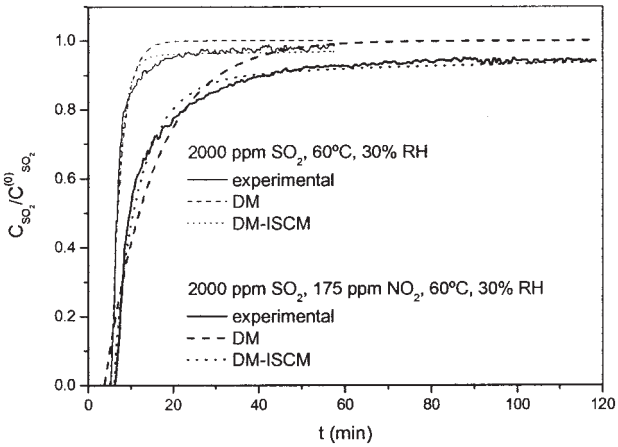

Figure 10. Experimental and fitted breakthrough curves to DM and DM-ISCM.

T on solid conversions can be observed, which is in agreement with the results reported by Ruiz-Alsop and Rochelle[2] and Krammer et al.[15] Furthermore, it can be observed that $C_{SO_2}/C^0_{SO_2}$ does not strictly achieve values of 1 in all the curves, especially in those corresponding to experiments at high RH (70%), which means that complete conversion has not been reached after 1 h of reaction. This observation seems to indicate that after a period of a sharp decrease of the reaction rate, the reaction would not stop and could proceed at a very low reaction rate.

As an instance of the effect of the presence of NO_2 in the reaction under study, two breakthrough curves of SO_2 are also included in Figures 5 and 6. It can be observed that NO_2 enhances the capability of $Ca(OH)_2$ for SO_2 recovery in the range of RH and NO_2 concentration indicated in Table 1. Furthermore, the presence of NO_2 seems to highlight the progress of the reaction at a low rate at long times in the range of conditions taken into account.

Concerning the effect of the SO_2 concentration on solid conversion, different behaviors can be observed depending on the RH (see Figure 7). Whereas a null influence is found at 30% RH, as was previously found,[2,15,16] a slight negative effect is found above 30% RH.

Results of solid analyses

Some XRD analyses identified $CaSO_3 \cdot (1/2)H_2O$ as the only product of the reaction. When the reaction took place in the presence of NO_2, however, $CaSO_4 \cdot (1/2)H_2O$ and $CaSO_4 \cdot 2H_2O$ were also detected. In all cases, the product seems to be well dispersed over the entire surface, as was confirmed by some EDS (energy-dispersive spectroscopy) analyses done in particles visualized by SEM and TEM. Significant amounts of sulfur have been detected at all the particle areas analyzed. However, the analyses showed that the solid product is not uniformly deposited onto the surface because the intensity ratio of the sulfur and calcium peaks differ widely in the same agglomerate.

Examination of the reacted particles by SEM showed that the desulfurization reaction at RH $<$ 70% leaves their shape and surface almost unchanged. However, as can be observed in Figure 8, the surface of the particles reacted $>$70% RH were covered by small grains, which generally showed a needlelike shape.

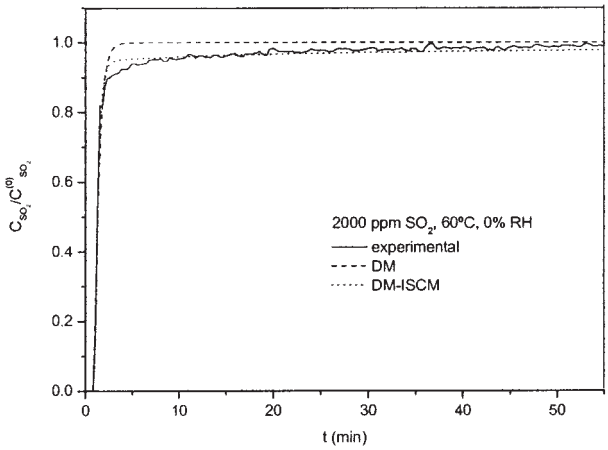

Figure 9. Experimental and fitted breakthrough curves to DM and DM-ISCM.

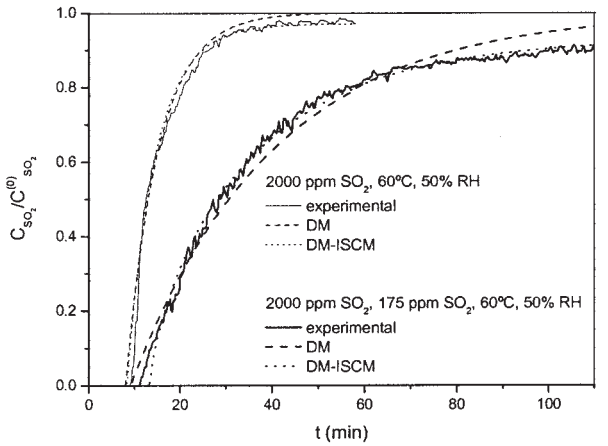

Figure 11. Experimental and fitted breakthrough curves to DM and DM-ISCM.

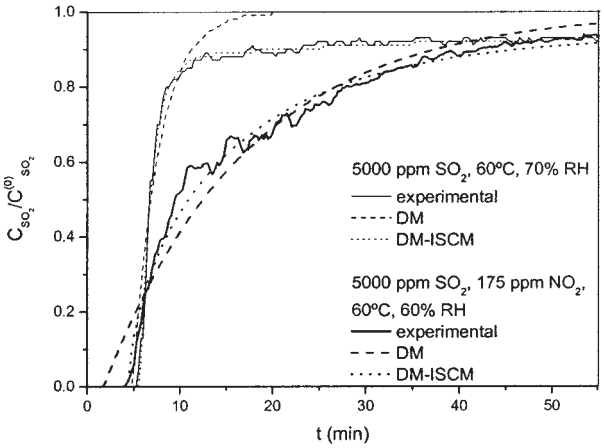

Figure 12. Experimental and fitted breakthrough curves to DM and DM-ISCM.

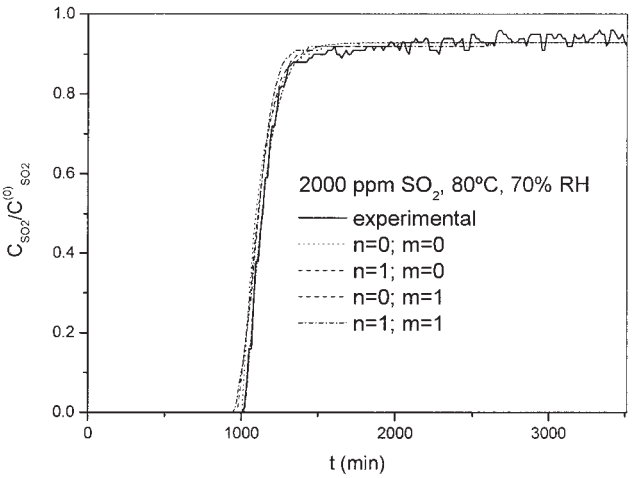

Figure 13. Experimental and fitted breakthrough curves to DM-ISCM.

Fitting of experimental breakthrough curves to the kinetic models proposed

Some examples of the fittings of the DM and DM-ISCM to the experimental breakthrough curves, both in the absence and in the presence of NO_2, are displayed in Figures 9–12. All the figures show that a DM-ISCM provides better fittings than a DM, which is confirmed by their lower values of calculated SQ (Table 4). The fittings of the parameters **n** and **m** corresponding to DM-ISCM show that in almost all experimental curves no significant differences have been found for the tested values of 0 and 1, as can be observed in the breakthrough curve plotted in Figure 13. The values of SQ included in Table 4 also confirm that the experimental results are not conclusive to discern between different values of **n** and **m**.

The effect of the RH on the parameters k_S, β, and $\bar{D}^P_{Ca^{2+}}$ are shown in Figures 14–16, respectively. As can be seen in Figure 14, the rate constant appears to be independent of RH at 40°C, whereas a positive influence of RH is detected beyond 40°C. Moreover, data from Figure 15 seem to indicate a decreasing exponential trend of the deactivation parameter β with the RH. Finally, the representation of $\bar{D}^P_{Ca^{2+}}$, with respect to the RH depicted in Figure 16, reveals a positive dependency of Ca^{2+} and HO^- solid-state diffusivities through the product layer on this parameter.

In Figures 14–16, some values of the adjustable parameters obtained from the experiments carried out in the presence of the NO_2 are also included. It can be observed that, although the presence of 175 ppm of NO_2 appears to moderately decrease the values of the rate constant, the parameters β and $\bar{D}^P_{Ca^{2+}}$ seem to be substantially reduced and increased, respectively. Furthermore, both the exponential trend of β with the RH and the positive influence of the RH on $\bar{D}^P_{Ca^{2+}}$ are highlighted.

Regarding the influence of temperature on the three parameters of the model, no clear trends have been found. Therefore, the reaction rate should be considered practically independent of temperature (see Figure 17), as has been already reported[15,16] in the range 50–90°C.

Discussion

Even though a DM proposed by Ho et al.[26] seems to predict reasonably well the rupture points and the sharp slope of the curves, the introduction of an ISCM appears to be necessary to fit them at long times, obtaining excellent agreements in such cases. Excluding values of 0% RH, calculated values of initial reaction rate in terms of dX_S/dt are in the range 3.5×10^{-4} to 1.7×10^{-3} s^{-1}, which corresponds to the range found experimentally by Klingspor et al.[27] ($0–2 \times 10^{-4}$ s^{-1}, depending on the RH) and by Krammer et al.[15] (around 10^{-2} s^{-1} for all the RH values tested).

A mechanism that might be consistent with the proposed kinetic model and that could explain the relevant role of water

Table 4. SQ of the DM and DM-ISCM Fitting

% RH	T (°C)	C_{SO2} (ppm)	C_{NO2} (ppm)	Reaction Time (h)	SQ of DM	SQ of DM-ISCM			
0	60	2000	0	1	0.23	0.04			
30	60	2000	0	1	0.29	0.08			
30	60	2000	175	2	1.86	0.18			
50	60	2000	0	1	0.17	0.10			
50	60	2000	175	2	0.70	0.14			
70	60	5000	0	1	1.41	0.04			
60	60	5000	175	1	0.56	0.15			
					SQ of DM-ISCM				
					$n = 0$; $m = 0$	$n = 1$; $m = 0$	$n = 0$; $m = 1$	$n = 1$; $m = 1$	
70	80	2000	0	1	0.066	0.052	0.049	0.061	

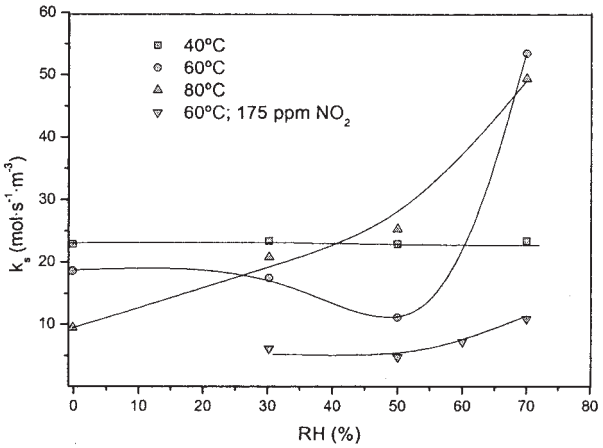

Figure 14. Influence of RH on k_S at 2000 ppm SO_2.

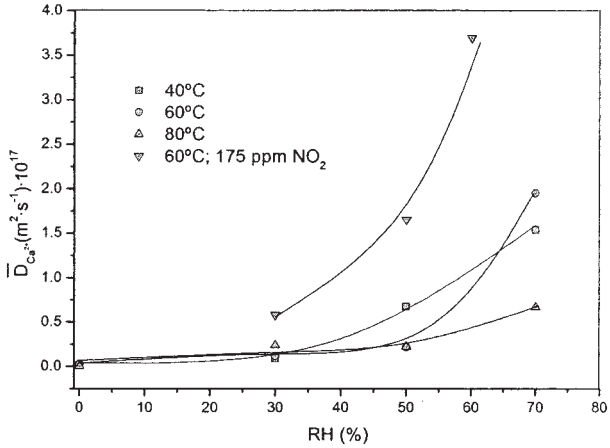

Figure 16. Influence of RH on $D^S_{Ca^{2+}}$ at 2000 ppm SO_2.

on the kinetics of the reaction would consist of the following stages (see Figure 18):

(1) Adsorption of water on the surface of the solid (pores and external).

(2) Adsorption of SO_2 on the surface of the solid and hydration to form a complex $SO_2{\cdot}nH_2O$ in the same way as indicated by Klingspor et al.[27]

(3) Outward diffusion of Ca^{2+} and HO^- ions from the $Ca(OH)_2/CaSO_3{\cdot}(1/2)H_2O$ interface to the outer surface, just when a layer of product has been built and the surface of $Ca(OH)_2$ has been deactivated.

(4) Reaction of $SO_2{\cdot}nH_2O$ with HO^- ions on the solid interface to produce sulfite ions and more water, as follows

$$SO_2 \cdot nH_2O + 2HO^- \rightarrow SO_3^{2-} \cdot (n-1)H_2O + 2H_2O \quad (15)$$

(5) Precipitation of $CaSO_3{\cdot}(1/2)H_2O$ by means of the following reaction

$$SO_3^{2-} \cdot (n-1)H_2O + Ca^{2+} \rightarrow CaSO_3 \cdot (1/2)H_2O \downarrow + (n-3/2)H_2O \quad (16)$$

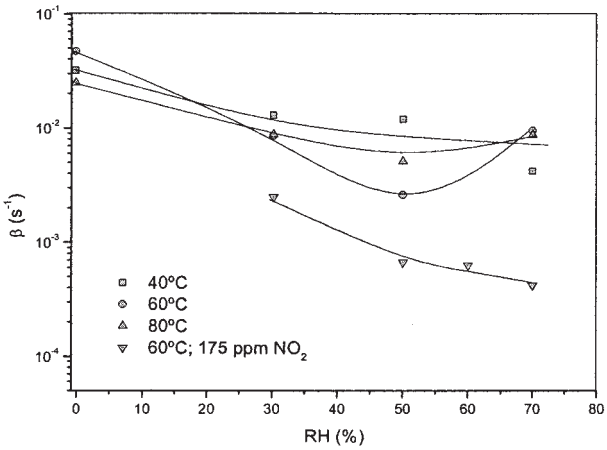

Figure 15. Influence of RH on β at 2000 ppm SO_2.

This mechanism does not correspond exactly to the one proposed for the reaction of SO_2 with lime slurries, because the number of expected water monolayers is <2.5 for RH $< 78\%$, as previously indicated at 70°C.[27]

According to this mechanism, a physical interpretation for the adjustable parameters β, k_S, and $\bar{D}^P_{Ca^{2+}}$ of the model can be proposed. The deactivation constant β can be regarded as a structural parameter because it should be related to the distribution of the layer of product on the surface of the reagent in the progress of the reaction; the rate constant k_S can be considered to be basically dependent on the hydration of SO_2 on the surface of the reagent; and $\bar{D}^P_{Ca^{2+}}$ is the diffusion of hydrated Ca^{2+} ions through the product layer and should account for the solid-state ionic diffusional contribution on the kinetics of the reaction. According to these considerations, the effect of RH observed in all parameters can be explained as follows:

Effect on k_S. As RH increases, a greater amount of water may be adsorbed on the surface of the solid, which should lead to a higher retention of SO_2 and to an increase of k_S.

Effect on β. The value of β decreases as RH increases. This behavior could be ascribed to the way the reaction product deposits on the surface of $Ca(OH)_2$, as shown in Figure 4. At low values of RH, the product covers the surface more uniformly, whereas at higher values the product builds up more clusterlike, as postulated by Krammer et al.[15] These results might be explained by the formation of a nonrigid aqueous layer on the solid surface at a high RH, which could allow small product crystals to move on the surface and to aggregate one to another, to achieve more stable structures by the reduction of the interfacial area between the solid reagent and the product. Consequently, a net active surface of $Ca(OH)_2$ would be generated, available for further reaction. This postulation is supported by Allen et al.,[39] who found experimental evidence of the reorganization of $NaNO_3$ layers on the surface of NaCl into separate microcrystallites of $NaNO_3$ on the NaCl crystal host, by means of TEM analysis, when the solid samples were exposed to 45–71% RH. Moreover, Zangmeister et al.[40] also found a rearrangement of $NaNO_3$ layers to form well-defined $NaNO_3$ "towers," when they used AFM (atomic force microscopy) to study the effect of a water-saturated atmosphere on the surface of NaCl (100) single crystal previously reacted with HNO_3.

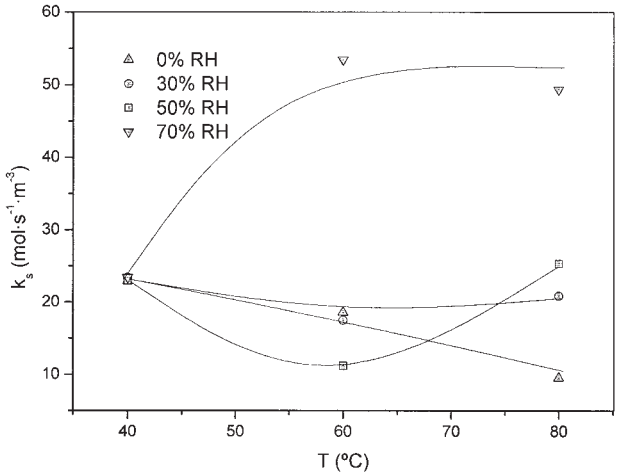

Figure 17. Influence of T on k_S at 2000 ppm SO_2.

Effect on $\bar{D}^P_{Ca^{2+}}$. The RH enhances the value of $\bar{D}^P_{Ca^{2+}}$. As the RH increases, the amount of water adsorbed in the product layer would also increase, implying that water improves the ionic movement through it because of the better stabilization of migrating ions.

The aforementioned positive effect of NO_2 on the kinetics of the reaction could be related to the formation of $Ca(NO_3)_2$ and $Ca(NO_2)_2$ species as products of its reaction with $Ca(OH)_2$. Because nitrates and nitrites are very hygroscopic compounds, the amount of water retained on the solid surface at a specific RH would be increased. Thus, the trends underlined for the parameters β and $\bar{D}^P_{Ca^{2+}}$, with respect to RH, would be stressed. However, a slight negative effect for the parameter k_S is observed, which could be explained by means of the competition between SO_2 and NO_2 for their adsorption on the surface of the solid reagent.

The unclear dependency of parameters k_S and $\bar{D}^P_{Ca^{2+}}$ with temperature can be explained by means of two opposite effects: on one hand, they should be activated with temperature, but on the other hand, as the temperature increases, the amount of water adsorbed decreases, as has been reported[41] for the adsorption of water on $Ca(OH)_2$/fly ash sorbents, which could lead to a reduction in the values of k_S and $\bar{D}^P_{Ca^{2+}}$. As a result, depending on the contribution of each factor, a different evolution of these parameters with temperature would be expected.

The values of $\bar{D}^P_{Ca^{2+}}$ obtained from the fittings are in the range $0.004–3.70 \times 10^{-17}$ m^2 s^{-1}, including the values obtained from the experiments with NO_2. No available values of Ca^{2+} and HO^- solid-state diffusion coefficients ($D^P_{Ca^{2+}}$ and $D^P_{HO^-}$) through $CaSO_3 \cdot (1/2)H_2O$ at temperatures around 40–80°C have been found in the literature. Comparing these values with those reported for different Ca^{2+} ions,[42] which are around 3×10^{-20} m^2 s^{-1} at 900°C for different solid lattices, the values found in this work are higher, taking into account the thermal effect. The ionic diffusion is thought to be increased because of the effect of hydration, mainly through the grain boundaries, which could act as fast diffusion paths, given that the atomic structure of these defects is more open than that of the product lattice structure.

Conclusions

This study confirms that the reaction between SO_2 and $Ca(OH)_2$ at low temperature is greatly influenced by the RH;

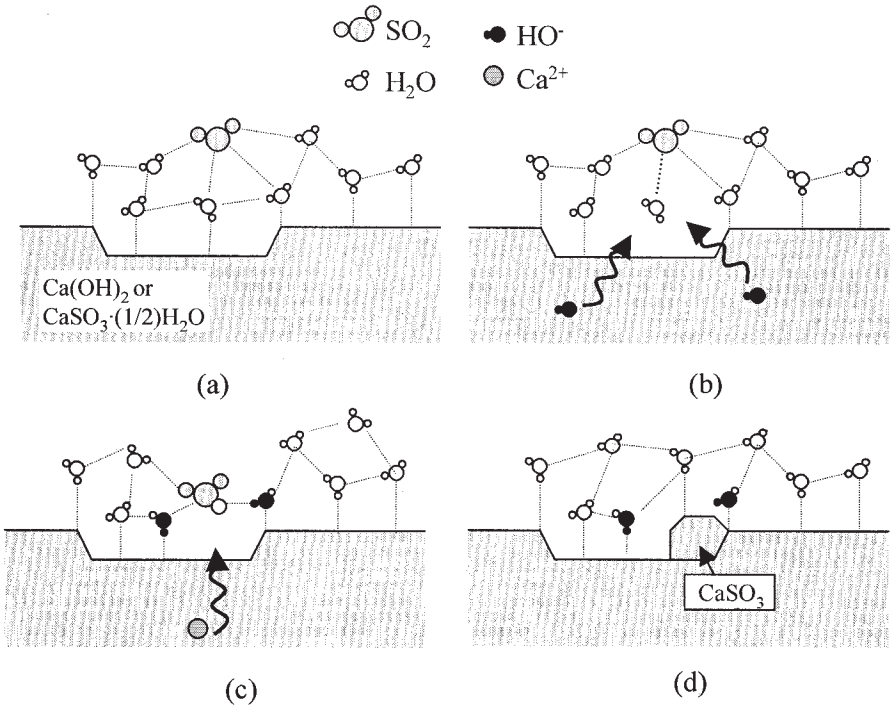

Figure 18. Reaction mechanism proposed for the formation of the $CaSO_3 \cdot (1/2)H_2O$.

(a) Formation of the complex $SO_2 \cdot nH_2O$; (b) outward diffusion of HO^-; (c) formation of $SO_3^{2-} \cdot (n-1)H_2O$ and two molecules of water by Eq. 10; outward diffusion of Ca^{2+}; (d) precipitation of $CaSO_3$ with the retention of 0.5 molecule of H_2O (Eq. 16).

meanwhile, the temperature and the SO_2 concentration seem to play a secondary role. Furthermore, the presence of NO_2 improves the recovery of SO_2, which can be explained by considering the formation of $Ca(NO_3)_2$ and $Ca(NO_2)_2$ hygroscopic salts.

The breakthrough curves obtained in a fixed-bed reactor show that the desulfurization reaction does not stop at long exposure times, but rather continues to proceed at very low reaction rates. The experimental curves were successfully simulated by a semiempirical kinetic model (DM-ISCM), which takes into account the reduction of the active surface of $Ca(OH)_2$, whereas the reaction progress is characterized by a solid-state outward diffusion of hydrated Ca^{2+} and HO^- ions from the inner $Ca(OH)_2/CaSO_3{\cdot}(1/2)H_2O$ interface to the outer $CaSO_3{\cdot}(1/2)H_2O$/gas surface. The role of water vapor in the kinetics of the system is reflected in the parameters of the model.

Acknowledgments

The authors express their gratitude to the Spanish government for financial support (CICYT projects AMB94-0200 and QUI98-0361). The authors are also thankful to Commercial and Industrial Aries, S.A. for the supply of the solid used in this study.

Notation

a = active surface
C_g = concentration of the gas in the bed, mol dm^{-3}
C^R_{Ca} = Ca^{2+} concentration in the crystalline lattice of $Ca(OH)_2$, mol dm^{-3}
d_p = diameter of inert solid particles, μm
D = diameter of the bed, m
DM = deactivation model
DM-ISCM = deactivation model combined with the inverse shrinking core model
$\bar{D}^P_{Ca^{2+}}$ = solid-state diffusion coefficient of Ca^{2+} ions, $m^2\ s^{-1}$
F = Faraday constant, 96485.3383(83) C mol^{-1}
$J_{Ca^{2+}}$ = surface flow of Ca^{2+} ions, mol $g^{-1}\ s^{-1}$
J_{HO^-} = surface flow of HO^- ions, mol $g^{-1}\ s^{-1}$
k_S = rate constant, $m^{3(n-1)}\ mol^{(1-n)}\ s^{-1}$
m = order of the deactivation process with respect to gas concentration
n = reaction order with respect to SO_2 concentration
M_S = molecular weight, g mol^{-1}
r = reaction rate, mol $g^{-1}\ s^{-1}$
R = radius of the particles, m
RH = relative humidity, %
S = surface area, $m^2\ g^{-1}$
SQ = sum of squares of residuals
X_S = solid conversion
z_i = electric charge of ion **i**

Greek letters

β = deactivation constant, $(dm^3\ mol^{-1})^m\ s^{-1}$
ε_L = porosity of the bed
ρ = density, kg m^{-3}
ν = rate of the gas in the bed, m s^{-1}
Φ, Ψ = kinetic parameters in Eq. 9
ϕ^P = electric field, V

Subscripts

S = solid
g = gas

Superscript

0 = inlet of the bed

Literature Cited

1. De Nevers N. Ingeniería de control de la contaminación del aire. Mexico City, Mexico: McGraw-Hill Interamericana Editores, S.A. de C.V.; 1998.
2. Ruiz-Alsop R, Rochelle GT. Effect of relative humidity and additives on the reaction of sulfur dioxide with calcium hydroxide. Prepared for Office of Research and Development. Washington, DC: U.S. Environmental Protection Agency; 1987.
3. Hartman M, Coughlin RW. Reaction of sulfur dioxide with limestone and the grain model. *AIChE J*. 1976;22:490-498.
4. Hartman M, Trnka O. Influence of temperature on the reactivity of limestone particles with sulfur dioxide. *Chem Eng Sci*. 1980;35:1189-1194.
5. Bardakci T. Diffusional study of the reaction of sulfur dioxide with reactive porous matrices. *Thermochim Acta*. 1984;76:287-300.
6. Borgwardt RH, Bruce KR. Effect of specific surface area on the reactivity of CaO with SO_2. *AIChE J*. 1986;32:239-246.
7. Sotirchos SV, Yu H. Overlapping grain models for gas–solid reactions with solid product. *Ind Eng Chem Res*. 1988;27:836-845.
8. Bhatia SK, Perlmutter DD. The effect of pore structure on fluid–solid reactions: Application to the SO_2–lime reaction. *AIChE J*. 1981;27:226-234.
9. Christman PG, Edgar TF. Distributed pore-size model for sulfation of limestone. *AIChE J*. 1983;29:388-395.
10. Simons GA, Garman AR, Boni AA. The kinetic rate of SO_2 sorption by CaO. *AIChE J*. 1987;33:211-217.
11. Suyadal Y, Oguz H. Dry desulfurization of simulated flue gas in a fluidized-bed reactor for a broad range of SO_2 concentration and temperature: A comparison of models. *Ind Eng Chem Res*. 1999;38:2932-2939.
12. Fan LS, Satija S, Kim BC, Nack H. Limestone/dolomite sulfation in a vertical pneumatic transport reactor. *Ind Eng Chem Process Des Dev*. 1984;23:538-545.
13. Doğu T. The importance of pore structure in the kinetics of gas solid non-catalytic reactions. *Chem Eng J*. 1981;21:213-222.
14. Orbey N, Doğu G, Doğu T. Breakthrough analysis of non-catalytic solid–gas reactions. *Can J Chem Eng*. 1982;60:314-318.
15. Krammer G, Brunner Ch, Khinast J, Staudinger G. Reaction of $Ca(OH)_2$ with SO_2 at low temperature. *Ind Eng Chem Res*. 1997;36:1410-1418.
16. Rochelle GT, White WG, Jozewicz W, Chang JCS. Reaction of hydrated lime with SO_2 in humidified flue gas. Paper presented at the 1990 SO_2 Control Symposium, New Orleans, LA, May; 1990.
17. Karatepe N, Ersoy-Meriçboyu A, Yavuz R, Kücükbayrak S. Kinetic model for desulphurization at low temperatures using hydrated sorbent. *Thermochim Acta*. 1999;335:127-134.
18. Garea A, Herrera JL, Renedo MJ, Fernández J, Irabien A. Thermogravimetric determination of the influence of water vapour in the FGD in-duct injection at low temperatures. *J Chem Technol Biotechnol*. 2000;75:484-490.
19. Yoon H, Stouffer MR, Rosenhoover WA, Statnick RM. Laboratory and field development of coolside SO_2 abatement technology. Proc of 2nd Annual Pittsburgh Coal Conference, September; 1985.
20. Aichinger G, Brunner Ch, Khinast J, Seebauer V, Staudinger G, Garea A, Fernandez I, Viguri JR, Irabien A. Kinetic studies on low temperature, dry flue gas desulphurisation. *Coal Sci*. 1995;1859-1862.
21. O'Dowd WJ, Markussen JM, Pennline HW, Resnik KP. Characterization of NO_2 and SO_2 removals in a spray dryer/baghouse system. *Ind Eng Chem Res*. 1994;33:2749-2756.
22. Nelli CH, Rochelle GT. Simultaneous sulfur dioxide and nitrogen dioxide removal by calcium hydroxide and calcium silicate solids. *J Air Waste Manage Assoc*. 1998;48:819-828.
23. Bausach M, Izquierdo F, Cunill F, Tejero J, Iborra M, Fité C. Semi-dry flue gas desulfurization: Study of the influence of the NO_2 as pollutant and $CaCl_2$ as additive. Proc of 9th Mediterrean Congress of Chemical Engineering, Barcelona, Spain; 2002.
24. Damle AS, Ramanathan K, Harmon DL. Kinetics of reaction between hydrated lime and sulfur dioxide. Proc of 6th Symp Transfer Utility Control Technology, EPRI CS-4918 (Vol. 1); 1986:18/1-18/20.
25. Irabien A, Cortabitarte F, Ortiz MI. Kinetics of flue gas desulfurization at low temperatures: Non-ideal surface adsorption model. *Chem Eng Sci*. 1992;47:1533-1543.
26. Ho C, Shih S, Liu C, Chu H, Lee C. Kinetics of the sulfation of $Ca(OH)_2$ at low temperatures. *Ind Eng Chem Res*. 2002;41:3357-3364.

27. Klingspor J, Strömberg AM, Karlsson HT, Bjerle I. Similarities between lime and limestone in wet-dry scrubbing. *Chem Eng Process*. 1984;18:239-247.
28. Ortiz MI, Garea A, Irabien A, Cortabitarte F. Flue gas desulfurization at low temperatures. Characterization of the structural changes in the solid sorbent. *Powder Technol*. 1993;75:167-172.
29. Schwartz CE, Smith JM. Flow distribution in packed beds. *Ind Eng Chem*. 1953;45:1209-1218.
30. Rase HF. *Chemical Reactor Design for Process Plants*. New York, NY: Wiley; 1977.
31. Doğu G, Doğu T. Kinetics of capture of sulfur dioxide and applications to flue gas desulfurization. NATO ASI Series E Applied Sciences 225. *Chemical Reactor Technology for Environmentally Safe Reactors and Products*. 1993:467-498.
32. Levenspiel O. *Chemical Reaction Engineering*. 3rd ed. New York, NY: Wiley; 1999.
33. Jorgensen C, Chang JCS, Brna TG. Evaluation of sorbents and additives for dry SO_2 removal. *Environ Prog.* 1987;6:26-32.
34. Hsia C, St. Pierre GR, Fan LS. Isotope study on diffusion in $CaSO_4$ formed during sorbent-flue-gas reaction. *AIChE J.* 1995;41:2337-2340.
35. Girifalco LA. *Atomic Migration in Crystals*. 1st ed. New York, NY: Blaisdell; 1964.
36. Philibert J. *Atom Movements. Diffusion and Mass Transport in Solids*. Paris, France: Les Éditions de Physique; 1991.
37. Ginstling AM, Brounshtein BI. Concerning the diffusion kinetics of reactions in spherical particles. *J Appl Chem USSR*. 1950;23:1327-1338.
38. Himmelblau D. *Process Analysis by Statistical Methods*. New York, NY: Wiley; 1970.
39. Allen HC, Laux JM, Vogt R, Finlayson-Pitts BJ, Hemminger JC. Water-induced reorganization of ultrathin nitrate films on NaCl: Implications for the tropospheric chemistry of sea salt particles. *J Phys Chem*. 1996;100:6371-6375.
40. Zangmeister CD, Pemberton JE. In-situ monitoring of the NaCl + HNO_3 surface reaction: The observation of mobile surface strings. *J Phys Chem B*. 1998;102:8950-8953.
41. Liu C-F, Shih S-M, Lin R-B. Kinetics of the reaction of $Ca(OH)_2$/fly ash sorbent with SO_2 at low temperatures. *Chem Eng Sci*. 2002;57:93-104.
42. Landolt-Börnstein data collection. 5. Teil Bandteil b. Berlin: Springer-Verlag; 1968.

Manuscript received Jun. 3, 2004, and revision received Sep. 6, 2004.